THE JOURNAL OF PHYSICAL CHEMISTRY C

Article

Cite This: J. Phys. Chem. C XXXX, XXX, XXX-XXX

pubs.acs.org/JPCC

CO_2 Conversion in a Gliding Arc Plasmatron: Multidimensional Modeling for Improved Efficiency

G. Trenchev,[†] St. Kolev,[‡] W. Wang,[†] M. Ramakers,[†] and A. Bogaerts*,[†]

[†]Research Group PLASMANT, Department of Chemistry, University of Antwerp, Universiteitsplein 1, B-2610 Antwerp, Belgium

[‡]Faculty of Physics, Sofia University, 5 James Bourchier Boulevard, 1164 Sofia, Bulgaria

Supporting Information

ABSTRACT: The gliding arc plasmatron (GAP) is a highly efficient atmospheric plasma source, which is very promising for CO_2 conversion applications. To understand its operation principles and to improve its application, we present here comprehensive modeling results, obtained by means of computational fluid dynamics simulations and plasma modeling. Because of the complexity of the CO_2 plasma, a full 3D plasma model would be computationally impractical. Therefore, we combine a 3D turbulent gas flow model with a 2D plasma and gas heating model in order to calculate the plasma parameters and CO_2 conversion characteristics. In addition, a complete 3D gas flow and plasma model with simplified argon chemistry is used to evaluate the gliding arc evolution in space and time. The calculated values are compared with experimental data from literature as much as possible in order to validate the model. The insights obtained in this study are very helpful for improving the application of CO_2 conversion, as they allow us to identify the limiting factors in the performance, based on which solutions can be provided on how to further improve the capabilities of CO_2 conversion in the GAP.

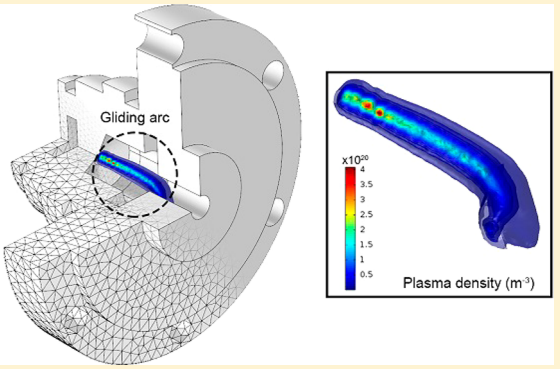

1. INTRODUCTION

There is an increasing interest toward using atmospheric plasma sources as gas conversion systems and specifically for converting CO_2 gas into value-added chemicals and new fuels.[1−6] Several different types of plasma sources have been tested already, and the energy efficiency varies for the different devices. The so-called reverse-vortex stabilized gliding arc (GA) reactor shows some of the best results.[7] Such a reactor combines the heat insulation principle of the reverse-vortex flow[1] with the reliability of a GA discharge.[5] The gliding arc plasmatron (GAP) utilizes this concept for achieving better conversion efficiency than common GA reactors.[7,8]

The GA is well-known plasma engineering. A high voltage (ac or dc) is applied between two flat, diverging electrodes, and a breakdown process in the gas leads to a plasma arc ignition at the shortest interelectrode distance, which then travels along the electrodes until it extinguishes. Then, a new arc is again created at the shortest interelectrode gap. A more classical example is the so-called Jacob's ladder. While being relatively simple and reliable, the conventional GA suffers from some problems in gas conversion applications. First, there is no practical way to force the gas to travel through the plasma arc, which is formed in a limited region between the flat electrodes, meaning that a large portion of the gas will just flow around it in the reactor without being converted. Second, the constant extinction and reignition of the arc leads to noncoherent gas treatment, which does not contribute well to the overall efficiency: the actual gas residence time inside the arc is very short.

One way to overcome these problems is to stabilize the arc by changing the design from flat electrodes to cylindrical electrodes, and to apply the gas flow tangentially instead of axially, giving rise to a vortex flow, and even a reverse-vortex flow, depending on the reactor design (see further). The vortex flow method of plasma stabilization has been widely used in different setups.[7−10] In essence, the gas is forced to flow along the walls in a vortex tube by two or more tangential inlets. If the inlets are placed on the same side of the tube as the outlet, the gas reaches the tube bottom and travels back in a smaller, inner vortex, hence reverse-vortex flow (RVF).[11] This design was proven to work well for a variety of plasma reactors, such as microwave,[10] inductively coupled plasma (ICP),[12] and GA.[7] The latter gains significant benefits from this method, as it solves the above-mentioned problems. The reverse-vortex mechanism essentially forces the gas to flow in the center, where the arc is located, instead of near the side walls; i.e., the walls are effectively insulated from convection heating. Moreover, the gas travels axially with respect to the arc, which promotes a higher residence time for the molecules in the actual discharge and improves the gas conversion. These

Received: August 25, 2017
Revised: October 18, 2017
Published: October 19, 2017

DOI: 10.1021/acs.jpcc.7b08511
J. Phys. Chem. C XXXX, XXX, XXX−XXX

effects were modeled and demonstrated for a conceptual GAP geometry in our previous work.[13]

In the present work, we model a practical GAP setup, which we also use experimentally for CO_2 conversion applications.[14] The exact device geometry is used as a modeling entity, which, while utilizing the same concept as in ref 13, has significantly different geometrical features. Furthermore, we use a more accurate turbulent flow model, i.e., the shear stress tensor (SST) model,[15] instead of the $k-\varepsilon$ model used in ref 13. In addition, the turbulent heat conductivity is taken into account using the Kays−Crawford model.[16] In first instance, we developed the model entirely in 3D with simplified argon chemistry to limit the computation time. On the basis of the insights obtained with this 3D model, we subsequently developed a 2D model which includes the complex CO_2 chemistry, adopted from ref 17. The entire model is developed with the COMSOL computational software package.[18]

In section 2 we describe the computational methods used for developing the gas flow and plasma models in 2D and 3D. Section 3 presents the obtained results, including the gas flow pattern, turbulent heat conductivity, arc movement, gas temperature, electron density, and temperature, as well as information on the CO_2 conversion, and we also compare some plasma properties with experiments to validate the model. The conclusion is given in section 4.

2. MODELING METHODS

2.1. Geometry. The gliding arc plasmatron (GAP) modeled in this work is based on the exact design, used experimentally,[14] and is shown in Figure 1. This design was developed by

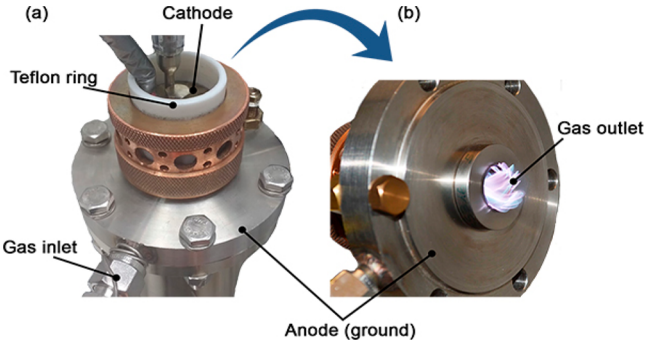

Figure 1. Photograph of the gliding arc plasmatron mounted on the gas tube (a) and detached, rotated 90° operating in free-air (b). The white Teflon insulator is visible—it is a sealing ring that encloses the cathode and acts as an electrical separator with the anode. It is not featured in the model, as it is an external entity with respect to the modeling geometry. The cathode can be seen on the top, with the cable and high voltage probe attached.

Rabinovich and co-workers at Drexel University.[7] It consists of a small RVF cylindrical chamber with two opposing cylindrical electrodes insulated with Teflon. This headpiece is typically mounted on a large tube, which is used to attach measurement instruments, such as a gas chromatograph and temperature sensors (see Figure 1a), but it can also be detached from this tube, and operated in open design, so that the arc movement can be visualized (see Figure 1b).

The RVF GAP module is quite versatile, and it offers different configurations, as both the cathode cap and the outlet anode are interchangeable for different flow configurations and outlet diameters. In the model, we only consider the internal structure, which can be seen in Figure 2. The reactor has six tangential inlets with a diameter of 1.6 mm and an axial outlet

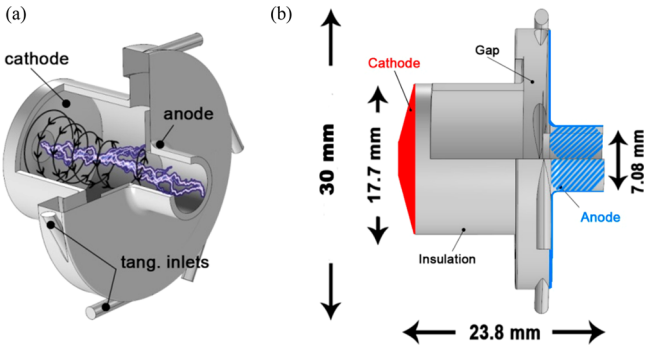

Figure 2. Internal structure of the reactor used for the model, with artistic representation of the arc. The reverse-vortex is indicated with black arrow lines (a). Side view of the internal structure (b). The domain length is 23.8 mm, and the swirl generator has a diameter of 30 mm. "Insulation" stands for a nonconductive boundary. The cathode is indicated in red and the anode in blue (striped).

with a diameter of 7.08 mm. The cathode (outlined in red, Figure 2b) is where the high voltage is applied. In the experimental reactor, the entire side wall is at cathode potential, and the initial discharge gap is the narrow area between the anode surface and this cathode sidewall (see "Gap", Figure 2b). However, in the plasma model, we consider only the back-end boundary as a cathode (red area, Figure 2b) in order to avoid plasma density and electron temperature errors at the sharp geometry edge near the "gap". Both cases were evaluated, and no difference was found in the plasma parameters. Indeed, once the arc is stabilized in the center, it is not in contact with the side walls, and the entire electrical current flows through the respective boundary where the arc is attached, i.e., the cathode cap in Figure 2.

2.2. Gas Flow Model. The gas flow is simulated in the entire internal 3D reactor geometry. The typical experimental flow rates are around 20 L/min, which corresponds to rather high internal flow speeds, in the range of 50−150 m/s. This will lead to strong turbulent oscillations, and if the modeling would be performed using the classical Navier−Stokes equations with direct numerical simulation (DNS), this would yield excessively long calculation times, for which supercomputers are required.[13,19] However, small-scale turbulent effects are out of scope of this study, as most of the computing power is dedicated to the actual plasma model. For this reason, we use a RANS (Reynolds-averaged Navier−Stokes) turbulent model, which significantly reduces the computational requirements by averaging turbulence over time. Nevertheless, the model is still accurate enough for the purpose of this study. We use the shear stress tensor (SST) model, which excels over most common turbulent models, like the $k-\varepsilon$ model.[13,18] This more advanced model solves the flow near the reactor walls more accurately and is more precise with turbulent variables, such as the turbulent viscosity, which affects the heat transfer. More importantly, the turbulent heat transfer is also included in the new model. Note that in ref 13 we used a $k-\varepsilon$ turbulent model to predict the flow field and the turbulent heat transfer was not included, but we will demonstrate here that it has a crucial effect on the gas temperature. The turbulent heat transfer model is based on the Kays−Crawford model.[16,18] The model inputs, such as gas flow rate and arc current, are adopted from

DOI: 10.1021/acs.jpcc.7b08511
J. Phys. Chem. C XXXX, XXX, XXX−XXX

our experiments,[14] in order to provide a solid ground for discussion and investigation. More information about the model can be found in the Supporting Information.

2.3. Turbulent Heat Transfer Model. In a gas medium, the temperature is determined by the gas thermal balance equation including a heat source. The equation is denoted as follows:

$$\rho C_p \frac{\partial T_g}{\partial t} + \rho C_p \vec{u}_g \cdot \nabla T_g - \nabla \cdot ((k_g + k_T)\nabla T_g) = Q \quad (1)$$

where C_p is the specific heat capacity of the gas, k_g is the temperature-dependent gas thermal conductivity (based on a material look-up table), k_T is the turbulent heat conductivity of the fluid, T_g is the gas temperature, and Q accounts for the gas heating due to elastic and inelastic collisions between electrons and heavy particles in the plasma.

The Kays−Crawford model[16,18] accounts for the resulting turbulent heat flux. It is solved for the turbulent Prandtl number, which is the ratio of the momentum eddy diffusivity and heat transfer eddy diffusivity. In this way, turbulence acts as an enhancement to the gas thermal conductivity through intense eddy mixing, resulting in a higher effective value for heat conduction for the conditions of the considered discharge; i.e., heat transfer is dominated by turbulent effects. More details can be found in the Supporting Information.

2.4. 3D Argon Plasma Model. The 3D plasma model is based on the simplified argon chemistry, presented in ref 13, in order to keep the computation time reasonable. This model was proven to be reasonably accurate and comparable with more complex chemistry models.[20] It is a fluid plasma model, built upon the assumption of a quasi-neutral plasma; i.e., ion and electron densities are equal.[21] The following equation is solved for the ion density:

$$\frac{\partial n_i}{\partial t} + \nabla \cdot (-D_i \nabla n_i + \mu_i n_i \overrightarrow{E_{amb}}) + (\vec{u}_g \cdot \nabla) n_i = R_i \quad (2)$$

where n_i stands for the ion density, μ_i stands for the ion mobility, $\overrightarrow{E_{amb}}$ is the ambipolar electric field, $\vec{u}_g$ is the gas flow velocity vector, D_i is the ion diffusion coefficient, and R_i stands for the ion production and loss rates due to chemical reactions. The electron density n_e is derived from the quasi-neutrality condition, which in this case is $n_e = n_i$ since only a single type of ion is considered in the model. Besides the above balance equation, a balance equation is solved for the Ar excited atoms as well as for the average electron energy. The model is described in more detail in the Supporting Information.

2.5. 3D−2D CO_2 Plasma Model. The plasma chemistry in CO_2 gas is much more complex. We present here an already reduced reaction set, adopted from ref 17−further reduction would lead to significant loss of accuracy for the given conditions. The chemistry set involves 40 species (see Table 1), 24 electron impact reactions, 19 ion reactions, and 7 vibrational transfer reactions. We put specific attention to the CO_2 vibrational levels, as they are stated to play an important role in energy-efficient CO_2 conversion in a GA.[17,22] Details about the vibrational levels included in our model can be found in refs 23−25.

Table 1. Overview of the CO_2 Plasma Species Included in the Model

ground state neutrals	CO_2, CO, C, O_2, O
charged species	e, CO_2^+, O_2^+, CO_3^-, O_2^-, O^-
excited species	CO_2 (25 vibrational states, 1 electronic excitation state), O_2 (3 vibrational states)

With this CO_2 chemistry, the computation time would be too long for a 3D model, as much more PDEs (partial differential equations) need to be solved for the particle balances. Furthermore, the complexity of the reactions increases the mesh requirements, as the density gradients for some of the species tend to be very strong. Thus, the model cannot work with the same settings as the 3D argon model. Therefore, we use a simplified 2D cutoff of the geometry. The flow pattern is directly interpolated into the 2D plane (see Figure 3) through interpolation functions in Comsol. The cutoff is essentially a plane of the 3D geometry, conserving all remaining geometrical features. The method is explained below. A detailed description of the chemical reactions in the CO_2 model is available in the Supporting Information.

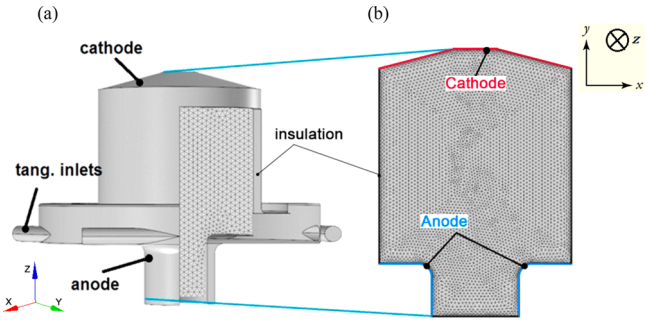

Figure 3. 3D reactor geometry (a) and the interpolated modeling plane in 2D (b), with indication of the computational mesh. See coordinate systems on the left (3D) and on the right (2D).

As can be seen in Figure 3, the 2D cut plane of the reactor is used as modeling entity, removing the swirl generator (tangential inlets), as no discharge takes place there. Accordingly, a fine 2D mesh is generated with 10 000 triangular elements and boundary layers. Thus, the red boundary becomes cathode and the blue−anode (see Figure 3b), as in Figure 2. The 3D flow vectors for "x" and "z" directions are translated to "x" and "y" directions in the 2D model. The "z" direction becomes just the length of the modeling plane and holds no gradients. This is the major limitation of the 2D approach: since the tangential motion (i.e., motion in the "z" plane) is not accounted for, the essential vortex pattern of the plasma cannot be captured. The flow pattern only features the sideways motion (from reactor periphery to center) and the outflow through the outlet (see Figure 4b). This is done by the use of interpolation tables within Comsol. With the same approach, the data for the turbulent heat conductivity is moved from the 3D to the 2D model.

3. RESULTS AND DISCUSSION

3.1. Gas Flow Pattern in Argon. The 3D gas flow stream lines, calculated with the SST model in argon gas, are presented in Figure 4. In Figure 4a, the stream line plot clearly depicts the formation of a reverse-vortex flow. The gas is forced into a tangential motion from the swirl generator (tangential inlets) and continues this trend through the reactor toward the closed cathode side at the end (= back of Figure 4a), after which it

DOI: 10.1021/acs.jpcc.7b08511
J. Phys. Chem. C XXXX, XXX, XXX−XXX

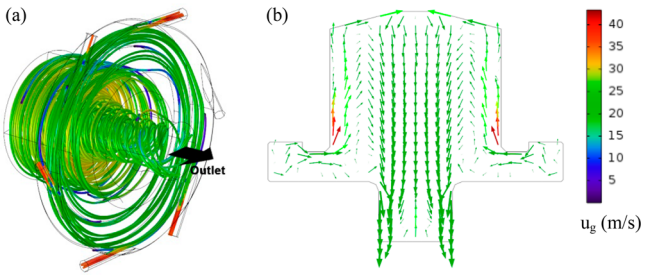

Figure 4. Stream line plot in 3D (a) and arrow surface plot in 2D (b) of the gas flow pattern, for an inlet gas flow rate of 22 L/min. The color scale at the right indicates the gas velocities in m/s and applies to both (a) and (b). Important note: the total velocity magnitude of all three vector components is expressed in the color scale in order to match the ranges of (a) and (b). However, in (b), the arrows represent only the axial and transverse directions, as the tangential motion (a) cannot be depicted in 2D.

moves in the opposite direction, in a smaller inner vortex toward the outlet. The details of the flow direction in a 2D plane of the reactor can be observed more clearly in Figure 4b, showing that the flow, when entering the reactor, first moves close to the sidewalls toward the top (= closed end of the reactor, i.e., cathode). Then, it returns and travels to the outlet in the opposite direction, forming a reverse-directed spiral, i.e., the reverse-vortex flow. The initial outer vortex takes place close to the walls due to the high inlet stream and moves at a high velocity (around 30−40 m/s). The inner reverse-vortex has a much lower velocity, which decreases toward the center, and it exits the reactor with a velocity magnitude around 20 m/s. This can be observed by the color scale in Figure 4.

A defining characteristic of the RVF is that the mass transfer takes place from the sides of the reactor to its center. This can be clearly seen by looking at the flow vectors in Figure 4b—the gas is transferred from the reactor periphery to the center, and it leaves the reactor through the outlet. The plasma reacts directly to this mechanism, as it is a part of the gas. In other words, when the gas stream is forced to the center, the plasma channel will also move to the center (due to convection; see convection term in eqs 1 and 2), and it will stay in this position as long as the gas keeps it stabilized. In this way, not only the plasma is effectively stabilized in the center but also the mass transfer is directed toward the center from all directions—meaning that the walls are thermally insulated from the hot plasma arc column. The fact that no heat is lost to the reactor walls or other parts of the reactor means that more power is consumed by the discharge; i.e., the plasma generation is more effective. Furthermore, keeping the walls insulated (cold) is also beneficial for the reactor materials itself. These results are consistent with the behavior shown in ref 13 and in other works on reverse-vortex flows.[1,7,11]

3.2. Argon Plasma Models. The obtained flow data in 3D are used directly as a stationary initial condition for the plasma model. The flow velocity is used in the convection term in the species balance equations (see Supporting Information), while the obtained values for turbulent heat conductivity are used as effective thermal conductivity in eq 1.

In Figure 5a, we illustrate the calculated plasma density, for an arc current of 240 mA, after a computation time of 5.3 ms, when the arc is stabilized in the center of the reactor. The plasma density is around 10^{20} m^{-3}. This value of 10^{20}−10^{21} m^{-3}

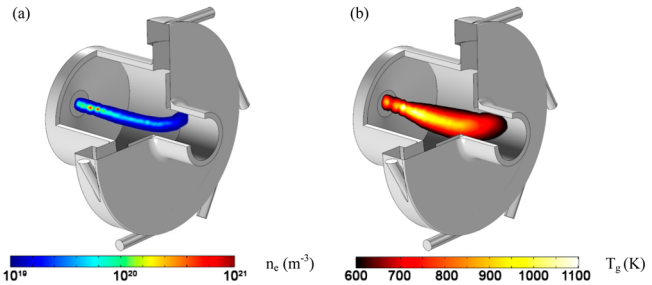

Figure 5. Plasma density [m^{-3}] (a) and gas temperature [K] (b) in the stabilized arc, depicted as iso-surface plots after 5.3 ms of computation time, for 240 mA of arc current and a gas flow rate of 22 L/min.

is typical for GA plasmas at atmospheric pressure.[1,26] The peak value does not change significantly during arc stabilization.

The calculated gas temperature (Figure 5b) at the same arc current of 240 mA is around 600−700 K at the sides of the arc, and it reaches 900−1100 K at the center, with a maximum of about 1100 K close to the cathode end, where the arc is slightly more contracted and the plasma density also reaches its maximum (see Figure 5a). These values are much lower than in our previous modeling study,[13] which is due to the inclusion of turbulent heat transfer (see section 2.3). The effective heat conductivity (see eq 1) is now a combination of the gas thermal conductivity (0.016 W/(m K) for argon at atmospheric pressure) and the computed turbulent heat conductivity, which accounts for heat transfer caused by the rapid turbulent oscillations in the flow. The computed value in the model is around 1−1.5 W/(m K) (see below), hence around 100 times higher than the value for the gas thermal conductivity, which was used in our previous model. This explains why the gas temperature is now much lower and more realistic. Indeed, taking into account the turbulent heat conductivity leads to a more distributed energy transfer in the gas and, thus, a lower maximum gas temperature.[27]

In order to demonstrate this effect in more detail, we show in Figure 6 the gas temperature in a 2D plot, calculated for the

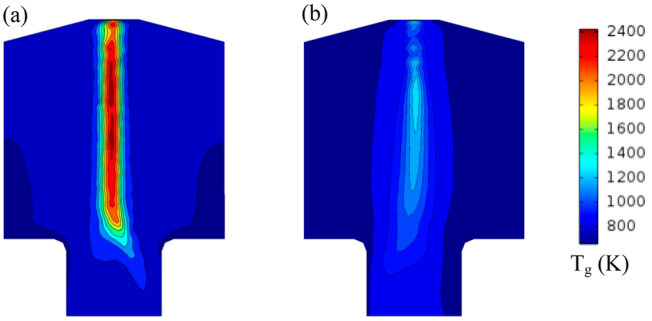

Figure 6. Gas temperature in the 3D argon model, without (a) and with (b) turbulent heat transfer, for the same conditions as in Figure 5. Gas inlets are omitted in the 2D projection.

same conditions as in Figure 5, both without and with including the turbulent heat conductivity. It is obvious that the temperature reaches a maximum value of 2400 K in the case without turbulent heat conductivity. Furthermore, the thermal profile of the arc column is now much narrower, i.e., with a diameter of only 2 mm (Figure 6a) vs 3−4 mm in Figure 6b because of the lower heat conductivity of the gas medium. This

DOI: 10.1021/acs.jpcc.7b08511
J. Phys. Chem. C XXXX, XXX, XXX−XXX

clearly illustrates the important role of turbulent heat conductivity in the GAP.

As the turbulent heat conductivity is anisotropic (see below), the arc temperature shows areas with higher and lower temperature, particularly in the area close to the cathode (Figure 5b). In addition, the higher heat conductivity leads to a wider thermal profile of the arc, as clearly shown in Figure 6. This effect has consequences for the plasma density as well (Figure 5a); i.e., gas turbulence has an influence on the entire arc structure.

In Figure 7, the time evolution of the arc position is illustrated in a 2D plane. The arc ignites at the periphery of the

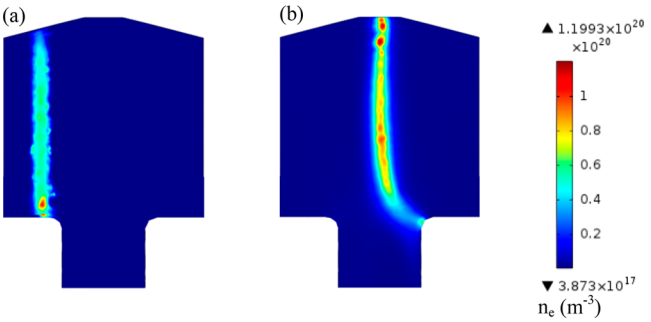

Figure 7. Arc position at 0.1 ms (a) and 5.3 ms (b) for the same conditions as in Figure 5. Gas inlets are omitted in the 2D projection.

reactor (Figure 7a) and gradually revolves in a spiral motion to the reactor center (Figure 7b). Then, it elongates toward the outlet and keeps rotating in a semistationary state (note the elongation in Figure 7). Note that the complex arc body cannot be completely depicted by a 2D cross section, as it is bent in all three directions. This process can be observed further in Figure 8, presenting the top view of the arc rotation. The arc body becomes a straight column but hook-shaped at the anode end. The revolution period is approximately 0.7 ms. We have also performed high-speed photography experiments of the arc rotation in our experimental reactor, showing a similar behavior and rotational speed.[28]

While the argon model provides valuable information on the discharge formation, the main purpose of this work is to model the GAP operating in CO_2. A complex CO_2 chemistry would yield excessive calculation times if using a 3D model. Hence, we need to develop this model in 2D. However, a 2D model raises some questions about its accuracy for describing the GAP. As mentioned, the first and most obvious difference is that there would be no gradients of plasma density or temperature in the "z" direction with respect to the modeling surface (refer to Figure 3). Second, the total arc current cannot be expressed in amperes, as there is no surface to integrate the current density upon—the cathode and anode boundaries are 1D lines. Therefore, the arc current can be expressed in A/m only. In addition, some convective cooling, coming from the tangential gas stream around the arc, is inevitably omitted, too.

To assess the effect of using a 2D model, we first developed the 2D model for argon, and we compared it with the 3D argon model results, before applying the 2D model for CO_2. In Figure 9, the effective heat conductivity for argon is moved from the 3D (a) to the 2D (b) model.

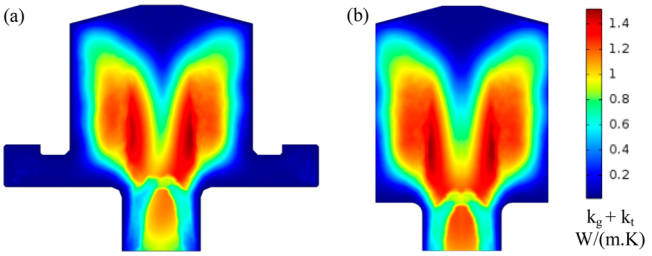

Figure 9. Effective heat conductivity (gas + turbulent) for argon in 3D (a) and interpolated in 2D (b).

Assuming that the arc has a cylindrical (or "wire") shape (judging from the 3D results), the total current in the 2D model can be approximated as follows. We assume that the current density in the "z" direction has the same distribution as in the "y" direction; i.e., the arc is symmetric. In this way, the current is obtained by integrating the current density over the arc region ($I = \int \sigma E 2\pi r \, dr$). This method has already been applied in ref 29 with satisfactory results.

In Figure 10, we show the results from the 2D argon model at the same conditions as in Figure 5 in order to compare with

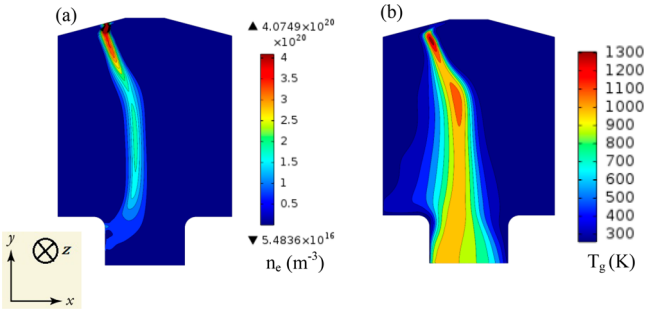

Figure 10. Plasma density (a) and gas temperature (b) in the 2D argon model, for the same conditions as in Figure 5.

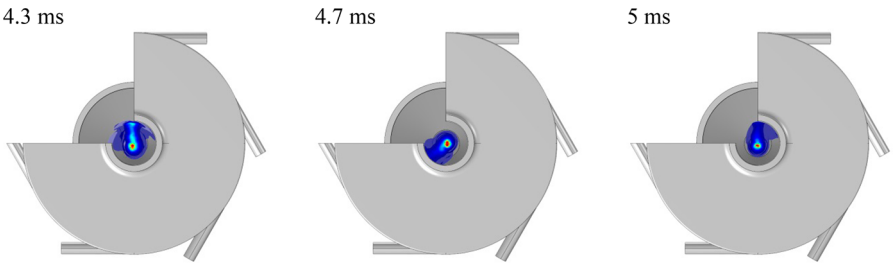

Figure 8. Arc position after stabilization in the reactor center, at 4.3, 4.7, and 5 ms (corresponding to one full rotation), for the same conditions as in Figure 5, illustrating how the rotating arc is attached at the anode end. A part of the anode body (at the top left) is removed, as done in Figure 5, to illustrate the inner part of the reactor.

DOI: 10.1021/acs.jpcc.7b08511
J. Phys. Chem. C XXXX, XXX, XXX−XXX

the 3D model results for model verification. Note that the geometry is a bit more simplified, neglecting the inlets and focusing only on the cylindrical reactor. At an estimated arc current of 240 mA (or current density in the 2D plane of 100 A/m), the plasma density calculated with the 2D model is in the same order of magnitude as in the 3D model, with 2×10^{20} m^{-3} in the arc center (cf. Figures 10a and 5a). The gas temperature shows rather good agreement with the 3D model (i.e., 1300 K vs 1100 K in 3D; cf. Figures 10b and 5b). Of course, the lack of convection cooling around the arc has an influence. In ref 29 the difference between the 3D and 2D model results was lower because the gas movement was dominantly in the same direction as the arc movement. The local increase of density and temperature at the top portion of the arc is visible in both the 2D and 3D model results and is due to a local drop in turbulent conductivity (see Figure 9). In general, from the good agreement between the 3D and 2D model results for argon, we can conclude that the 2D model provides a realistic picture of the GAP and can also be used to describe the GAP in CO_2. These results are presented in the next section.

3.3. 3D–2D CO_2 Model. The CO_2 model is a combination of a 3D gas flow model and a 2D plasma model. For the CO_2 turbulent heat conductivity, an additional 3D computation is carried out for CO_2 gas. This was done in order to account for the specific aspects of turbulence in the CO_2 gas. While the flow field for CO_2 is not significantly different from that of argon, the resulting turbulent heat conductivity is much higher (4–5 W/(m K)) due to the higher turbulent viscosity. Because of this, the plasma in CO_2 is subject to even more intense turbulent cooling. The turbulent heat conductivity and the flow field for CO_2 were included in the 2D CO_2 model in the same manner as described in section 3.2 by using interpolation tables.

The CO_2 model provides the same type of data as presented above for argon, but major differences in the actual results are to be expected due to some fundamental differences between argon and CO_2 plasmas. First, the different plasma chemistry leads to different excitation levels and power requirements. Therefore, the CO_2 plasma density (Figure 11a) is about an order of magnitude lower when compared to argon at similar conditions, i.e., with a maximum of 4×10^{19} m^{-3} in the arc center vs 4×10^{20} m^{-3} for argon (see Figure 10a). Similar reporting for GA plasma can be found in other works. Indeed, in ref 26 diagnostics were carried out on a classical air GA plasma, showing values for the plasma density of 10^{18}–10^{19} m^{-3} and for the vibrational temperature of 2600 ± 300 K in the nonequilibrium zone. A gas temperature of up to 4000 K was measured in ref 30 reporting a similar plasma density as well, i.e., 10^{18}–10^{20} m^{-3}, for an arc discharge with CO_2. In ref 31 a vibrational temperature of 3500 K is reported for air plasma.

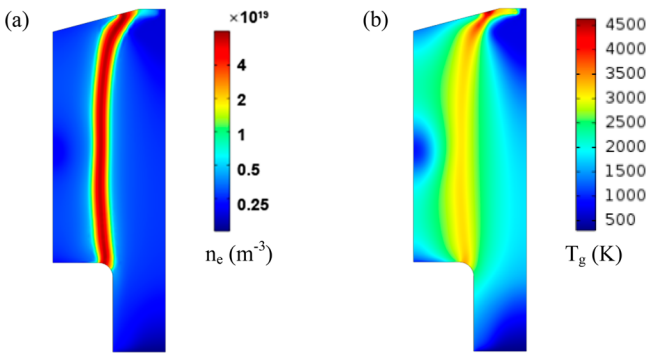

Figure 11. Plasma density (a) and gas temperature (b) at 100 A/m of current density in the CO_2 model, a gas flow rate of 22 L/min, and after a calculation time of 1 ms. The estimated total current is 240 mA. Note that only one-half of the cylindrical cross section is considered in this model to further limit the calculation time.

The reason for this difference in plasma density is because the applied power is also distributed to vibrational excitation and dissociation of the molecules in the case of CO_2, besides ionization and electronic excitation, which are the only possible inelastic electron-induced processes in argon. In other words, the CO_2 gas requires much more power to reach the same level of ionization in comparison with argon. The different plasma chemistry will alter the results even further. The numerous collisional reactions in the CO_2 plasma contribute more to the gas heating and result in a much higher value for the gas temperature (see Figure 11b). Furthermore, vibrational excitation, and subsequent vibrational–translational relaxation, which is an important gas heating mechanism in CO_2, is absent in argon. In the case of CO_2, the arc center, which is subjected to intense turbulent cooling, is characterized by a gas temperature of 3100 K (Figure 11b), while in the arc ends, where it is attached to the electrodes, an even higher value (4500 K) is reached, due to the lower turbulent heat conductivity in these areas. This behavior is similar to the 3D argon model results, where the arc temperature is also nonuniform, due to the influence of the anisotropic heat conductivity, but the values in argon are much lower (cf. Figures 11b and 5b).

It needs to be mentioned that the gas temperature value of 4500 K in the CO_2 model near the electrodes is actually quite high. The boundary condition for the reactor walls and electrodes is adiabatic in this model; i.e., no heat transfer can take place at these entities (see details in the Supporting Information and ref 13). This leads to an overestimation of the arc temperature near the electrodes. In a real-case scenario (classical or RVF GA), the electrodes are large pieces of metal, often connected to additional metal tubes for gas exhaust (see Figure 1) or a physical support. In such case, the heat will be distributed to the rest of the system. In addition, it has to be taken into consideration that this is the temperature of the plasma itself, which density is far lower than the density of steel, for example. This means that the total heat transfer to the electrodes will be rather low, and therefore well absorbed by the metal structure, without raising its temperature to the melting point. On the other hand, normal wear (i.e., microscopic melt points), especially on the cathode, occurs in our experiments due to the thermionic emission. So the gas temperature near the electrodes is to be viewed with caution, as it might be overestimated. Modeling a more detailed interaction between the arc and the electrodes is not possible at this point.

When taking the electrodes into consideration, another important remark needs to be given. The reactor operates in the "arc" regime of a dc atmospheric discharge. This means that the cathode surface features a hot (a few thousand degrees K) spot, which is a source of thermal electron emission and strong blackbody radiation. When measuring the total power input in the reactor, it has to be considered that a significant amount of it goes into cathode heating. Its amount will depend on a number of conditions. A sharp-edged electrode would promote a higher electric field and stronger emission (see reports on electric field in ref 13) but will also heat up and even melt, depending on the total current. The actual size and shape of the

DOI: 10.1021/acs.jpcc.7b08511
J. Phys. Chem. C XXXX, XXX, XXX–XXX

electrode and the properties of the metal (heat conductivity) will have an impact on the heat distribution and hence power draw. Last but not least, the work function of the particular metal used for the cathode can influence the conditions of forming a cathode spot. For this reason, when comparing electrical characteristics, it has to be mentioned that the cathode spot formation is not featured in the model.

Note that the arc in Figure 11 is not stabilized in the reactor center yet because the results are plotted at a time of 1 ms. However, at this time, the steady-state values of plasma density and gas temperature are reached already, as was demonstrated in ref 13; i.e., they would not change as the arc advances further into the reactor center. The reason that the arc is not shown in the center here is due to the fact that the centerline of the modeling plane holds a boundary condition that does not permit flux; i.e., with the arc at this position, the model would provide invalid results, as the boundary condition "no flux" will not permit the plasma in the center. For this reason, the arc is modeled only until it is still near the sidewall (corresponding to 1 ms of modeling time).

Figure 12 illustrates the electron temperature, gas temperature, and the vibrational temperature, determined from the

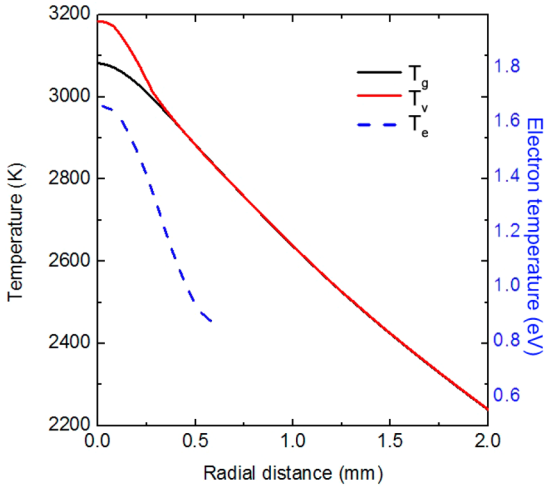

Figure 12. Gas (translational) temperature and vibrational temperature (determined from the first vibrational level) (in K; left axis) and electron temperature (in eV; right axis), in the arc, as a function of radial position from the arc center, for the same conditions as in Figure 11.

first vibrational level of CO_2, as a function of radial position from the arc center, for the same conditions as in Figure 11, at y = 15 mm and time = 1 ms. The electron temperature reaches a maximum of 1.6 eV in the arc center and drops to lower values after 0.5 mm distance, in correspondence with experimental data from literature for a GA in air.[26] As expected, this value is lower than the calculation result in argon (i.e., 2.5−2.6 eV[13]). The electron temperature is plotted up to 0.5 mm only, in order to omit the background heating temperature. The electron temperature value is much higher than the gas temperature and vibrational temperature (i.e., 1.6 eV or 18 500 K vs ca. 3000 K), indicating the nonequilibrium character of the GAP and explaining why it is very suitable for CO_2 conversion, as the electrons are energetic enough to activate the gas by ionization, excitation, and dissociation. The gas temperature shows a less steep drop as a function of radial position due to the high turbulent thermal conductivity. The difference between gas temperature and vibrational temperature is only around 100 K in the arc center, and both temperatures even become equal to each other after 0.25 mm from the center. This difference between vibrational temperature and gas temperature is lower than what was calculated in ref 17. The reason for this difference is the higher current density, and thus energy input of the discharge, at the conditions under study. The fact that the vibrational temperature is so similar to the gas temperature indicates that the vibrational distribution function (VDF) of CO_2 is close to thermal and that the higher vibrational levels of CO_2 are not really overpopulated, which would be needed for energy-efficient CO_2 conversion. Thus, although CO_2 conversion proceeds already in an energy-efficient way in a GAP,[7,14] our model calculations reveal that the energy efficiency could be further improved when the vibrational kinetics could be further exploited.

Figure 13 presents the number density of different neutral species in the plasma region, as a function of position from the

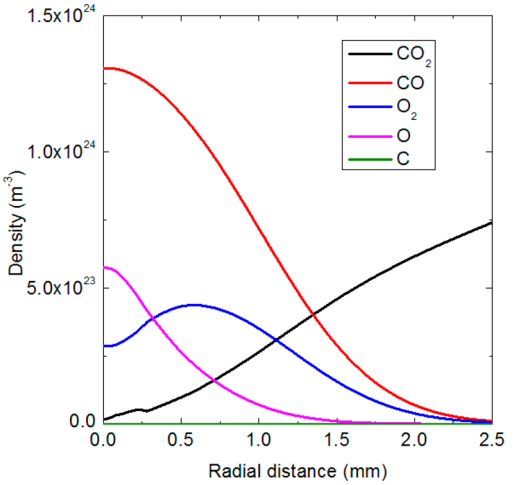

Figure 13. Number density of the various neutral species in the arc as a function of radial position from the arc center, for the same conditions as in Figure 11.

arc center, for the same conditions as in Figure 11. The conversion of CO_2 into CO (and O/O_2) is evident: The neutral CO_2 density shows a clear drop in the arc center, down to 10^{22} m^{-3} in the periphery of the arc, and even below in the arc center, indicating almost complete conversion. Clearly, apart from CO_2 splitting upon electron impact collisions, a significant thermal conversion takes place. This can also be deduced from the obtained gas temperature: the thermal conversion can reach 70% with a gas temperature above 3000 K.[6] High gas temperatures actually contribute well to the overall conversion. This complete conversion is, however, only limited to a very narrow arc region, while the rest of the CO_2 gas traveling through the reactor is not being converted (or only to a limited extent, due to thermal conversion when it comes in close contact with the arc). Moreover, it is of crucial importance how the gas approaches the discharge zone: molecules moving axially with respect to the arc will be exposed to the plasma for a longer time period, in comparison to molecules entering from the sides or swirling around in the vortex. Therefore, the overall CO_2 conversion in the GAP will be significantly more limited; i.e., we measured values in the order of 5−10%.[14] Overall, the problem can be viewed as a two-

DOI: 10.1021/acs.jpcc.7b08511
J. Phys. Chem. C XXXX, XXX, XXX−XXX

phase gas mixing process, where a (virtually) untreated gas mixes with a chemically active discharge.

In Figure 14, the total number density of all species in the reactor is plotted as a function of radial distance to the arc

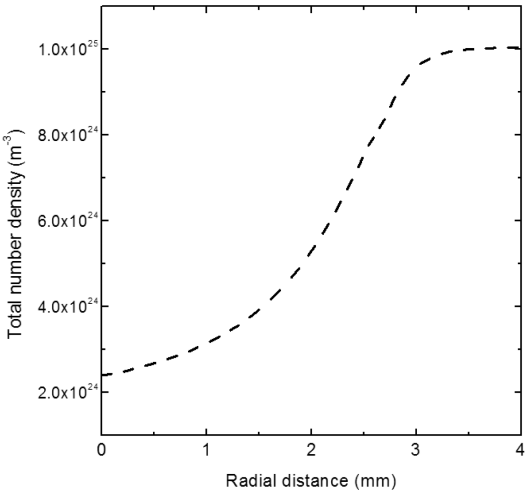

Figure 14. Total number density of all species as a function of radial position from arc center.

center, showing the inverse relationship with the gas temperature, following the ideal gas law.

Thus, while the RVF configuration causes the discharge to be stabilized in the center of the reactor, and forces the gas to travel axially with respect to the plasma arc, not all the gas passes through the discharge zone: a significant amount still leaves the reactor without being in touch with the plasma. In fact, this amount varies across the discharge itself: the arc becomes wider near the reactor outlet, resulting from a combination of flow effects, gas expansion, and heat conductivity. The gas velocity magnitude is much higher at the outlet walls than in the central arc itself (see Figure 4). Also, the flow velocity varies across the arc length, which complicates the estimation further. In order to gain some insight into the problem, the flow rate of gas through the arc body is evaluated. In Figure 15, the flow velocity is integrated over the arc cross section, yielding the flow rate at several positions in the axial

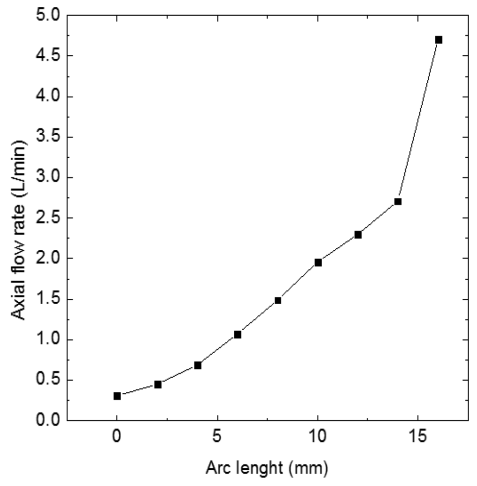

Figure 15. Axial flow rate through the arc cross section for the same conditions as in Figure 11. Inlet flow rate: 22 L/min.

direction, i.e., along the arc length—from the cathode surface to the outlet. Notice that the flow rate varies across the entire arc body, ranging from 0.3 to 5 L/min.

Averaging the values in Figure 15 gives an average flow rate through the arc body of 1.74 L/min. From Figure 13 we can assume 100% conversion within the arc itself, so we can conclude that the actual conversion would correspond to the percentage of flow moving through the arc. It should be noted that this is an ideal case, with extremely fast quenching, in order to avoid the recombination of CO and O/O_2 back to CO_2. Comparing the average flow rate of 1.74 L/min passing through the arc body to the total gas flow rate of 22 L/min at the inlet indicates that 8% of the gas is forced axially through the arc and is completely converted. This corresponds well with the experimental values of the CO_2 conversion obtained in our GAP, which tend to be between 5% and 8% (see Figure 16).[14]

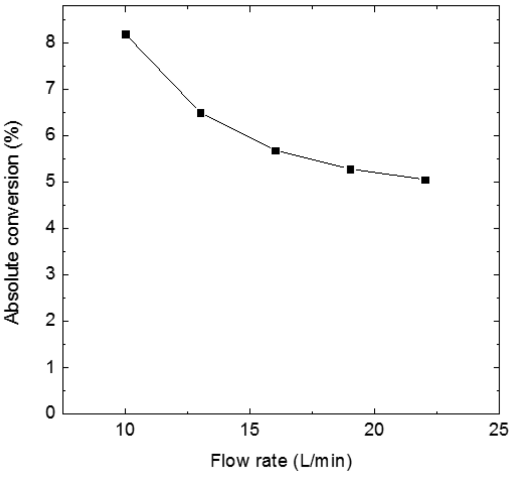

Figure 16. Measured absolute conversion of CO_2 at different flow rates, for reactor power of 500 W, adopted from ref 14.

The values below 8% are explained because in reality some recombination of CO and O/O_2 back into CO_2 will take place as well (i.e., nonideal case; see above). It is clear that a longer arc would increase the discharge flow capacity and yield better results. Increasing the total input flow rate would increase the arc throughput as well, but on the other hand, the residence time for the molecules will drop, lowering the overall conversion, as can be observed from Figure 15.

Another way of improvement would be to increase the turbulent mixing and conductivity, which would lower the gas temperature. By doing so, the reverse reaction, i.e., the three-body recombination reaction of CO with O into CO_2, can be avoided to some extent, improving the net conversion and the energy efficiency. Note that this three-body reverse reaction of CO + O + M one of the predominant reactions for CO_2 formation, along with $O_2 + CO \rightarrow CO_2$.[17] Moreover, a lower gas temperature will cause less vibrational−translational relaxation, which is an effective loss mechanism for the higher vibrational levels. Hence, this lower temperature will allow to better exploit the vibrational kinetics through an over-population of the higher vibrational levels, which are crucial for energy efficient CO_2 conversion. On the other hand, a higher temperature also gives rise to thermal conversion, which contributes to the overall conversion, but it will not be able to pass the thermal equilibrium limit. The latter is definitely possible by the nonthermal conversion induced by electrons

DOI: 10.1021/acs.jpcc.7b08511
J. Phys. Chem. C XXXX, XXX, XXX−XXX

and the vibrational CO_2 levels, which is the strength of plasma-based CO_2 conversion.[6] It has indeed been shown before that the gas temperature plays a key role in the energy efficiency for CO_2 conversion in so-called warm plasmas, such as GA discharges and microwave plasmas, and in general, lower temperatures yield a more energy efficient conversion.[32] Therefore, the discharge temperature control is of utmost importance for the reactor efficiency.

Increasing the turbulent mixing, to lower the gas temperature, can be achieved by increasing the flow rate or changing the characteristic dimensions of the reactor (i.e., inlet/outlet diameter, reactor body size, etc.). In addition, the total arc power has a clear influence on the gas temperature, but in practice its adjustment range is limited due to the power source and the arc regime specifics (i.e., the arc plasma requires a high current and results in a rather low discharge voltage, in comparison with a glow regime, for instance).[14]

4. CONCLUSION

In this work, we present a very first model for a RVF GA reactor for CO_2 conversion. Because of the high computational cost, the study is composed by separate 3D and 2D models—a 3D argon gas flow and 3D argon plasma model as well as a 3D CO_2 gas flow and 2D CO_2 plasma model. The 3D argon model operates with a simplified chemistry set for argon and is focused on the gas dynamics, the arc movement, and the basic plasma characteristics of a GA in RVF configuration, such as plasma density and temperature. The calculated plasma density and gas temperature in argon are around 10^{20} m^{-3} and 1100 K, respectively, and these values are comparable to the available literature.[1,11,26] We also clearly demonstrate the arc rotation and stabilization mechanism through elaborate 3D observations. This work is a substantial improvement of ref 13 due to the usage of a realistic (and not just a conceptual) geometry, the total arc current lying within the experimental range, and especially the turbulent heat transfer calculation.

The insulation mechanism is clear: the RVF reactor forces the mass flow from the walls in the direction to the arc; i.e., the walls can only receive minor heating by radiation from the arc, but not through convection or conduction. The major effect of the turbulent heat transfer on the calculated gas temperature is demonstrated by comparing with calculation results where this was not yet included. The high flow turbulence in the reactor leads to intense heat exchange due to rapid turbulent oscillations. The effect is dominant for the arc cooling—the turbulent gas thermal conductivity for the given conditions is almost 100 times higher than the gas thermal conductivity. This leads to a much wider thermal profile of the arc, a difference in arc contraction, and a significantly lower gas temperature. As far as we know, this effect has not been demonstrated so far in low-temperature arc plasma models.

Applying the model to a CO_2 plasma indicates that the CO_2 conversion is partially through electron impact activation and partially thermal. Indeed, the gas temperature is around 3000 K, hence a factor 3 higher than in argon, because of the more collisional plasma and in particular by the gas heating due to vibrational excitation of CO_2, following by vibrational−translational relaxation. Our model also shows that in spite of the high gas temperature the arc is certainly not in thermal equilibrium, in agreement with other papers,[26,30,31] as the electron temperature is still a factor 6 higher than the gas temperature. However, the vibrational temperature is quite close to the gas temperature, and we believe that the energy efficiency of CO_2 conversion in the RVF GAP, although being very promising already (∼30−35%[14]) can be further improved if the nonequilibrium character of the vibrational distribution function can be further exploited. Effects of the turbulent cooling may have a significant impact on this property because vibrational−translational relaxation, which is the major loss mechanism for the higher vibrational levels, will be reduced at lower temperature. That is the reason why we stress its importance in this paper. A lot of emphasis in this paper is put on the argon models in 2D and 3D, while the main object of interest is the CO_2 plasma. There is a good reason for this—argon and CO_2 plasmas are fundamentally different. They feature different plasma properties, gas temperature, and discharge structure. As the CO_2 plasma model is within reach only in 2D models, there is no way to predict whether it will retain the same properties in 3D. For this reason, the approach of "downgrading" a 3D argon model into 2D, and comparing them, was used to validate the accuracy of the method: as the difference between the 3D and 2D argon models is acceptable, we therefore conclude that the 2D CO_2 model provides data with a reasonable accuracy. In this way, we have extracted the most of the currently available methods and their limitations.

Finally, we also calculated the densities of the CO_2 splitting products, i.e., mainly CO, O_2, and O, and we demonstrated that the CO_2 conversion in the center of the arc is virtually 100%. The reason that the overall CO_2 conversion is so much lower in our experiments is because only a limited fraction of the gas passes through the actual discharge. We evaluated the overall conversion through detailed analysis of the flow configuration, predicting that the gas flow through the arc is only about 8% of the total gas flow at the inlet. This means that the overall conversion is also limited to (at maximum) 8%, which is in excellent agreement with our experimental findings.

While these models can already provide a lot of important information, they still lack some specific features. First, the electrode surface is not accounted for. As mentioned, microscopic bumps and scratches on the electrodes cause a local increase of the electric field and thus attract the arcs. In reality, the arc movement is much more random, while the model shows a smooth transition of the arc position. Also, the adiabatic boundary condition for the electrodes is an approximation of the model. This has been already discussed in our previous work.[13] The lack of description for the electrode heat balance omits the ability of the model to perform calculations for thermionic emission on the cathode "hot spots" or emission zones. Furthermore, the 3D−2D CO_2 approach also has its limitations: with the arc being a plane instead of a "string", there is no easy way to measure what portion of the gas mixes with the discharge and can be converted. The gas cannot swirl around the arc, bend it in a spiral shape, or flow around it, as it would do in the 3D model and the experiments. Therefore, for predicting the fraction of gas passing through the arc, we used the insights obtained from the argon 3D model.

In summary, the study presented here makes the most out of the available plasma modeling methods. A complete 3D quasi-neutral model for argon plasma describes the arc motion in detail and incorporates advanced turbulence modeling for turbulent heat transfer. A CO_2 model, which uses a combined approach—flow and turbulence calculations in 3D and plasma model calculation in 2D—describes the complex plasma chemistry and its impact on CO_2 conversion. With this foundation, the path is clear: we have a clear definition of the arc shape and its movement, its plasma parameters in CO_2 gas,

DOI: 10.1021/acs.jpcc.7b08511
J. Phys. Chem. C XXXX, XXX, XXX−XXX

and its conversion rate, based on which we plan to develop in the future a complete computational study of the conversion and energy efficiency, involving more complex flow modeling, featuring particle tracing.

■ ASSOCIATED CONTENT

Supporting Information

The Supporting Information is available free of charge on the ACS Publications website at DOI: 10.1021/acs.jpcc.7b08511.

A detailed description of the gas flow and plasma model (PDF)

■ AUTHOR INFORMATION

Corresponding Author

*E-mail: georgi.trenchev@uantwerpen.be (A.B.).

ORCID

G. Trenchev: 0000-0002-0359-4858

M. Ramakers: 0000-0001-7145-3398

Notes

The authors declare no competing financial interest.

■ ACKNOWLEDGMENTS

This research was funded by the Fund for Scientific Research Flanders (FWO; Grants 11U5316N and G038316N) and the European Marie Skłodowska-Curie Individual Fellowship "GlidArc" within Horizon2020 (Grant 657304). The GAP was developed by Alexander Rabinovich et al. at Drexel Plasma Institute (Patent WO2011119274A1).

■ REFERENCES

(1) Fridman, A. *Plasma Chemistry*; Cambridge University Press: New York, 2008.

(2) Wang, Q.; Shi, H.; Yan, B.; Jin, Y.; Cheng, Y. Steam enhanced carbon dioxide reforming of methane in DBD plasma reactor. *Int. J. Hydrogen Energy* **2011**, *36*, 8301−8306.

(3) Tao, X.; Bai, M.; Li, X.; Long, H.; Shang, S.; Yin, Y.; Dai, X. CH_4-CO_2 reforming by plasma − challenges and opportunities. *Prog. Energy Combust. Sci.* **2011**, *37*, 113−124.

(4) Bogaerts, A.; Kozak, T.; Van Laer, K.; Snoeckx, R. Plasma-based conversion of CO_2: Current status and future challenges. *Faraday Discuss.* **2015**, *183*, 217−232.

(5) Tu, X.; Whitehead, J. C. Plasma dry reforming of methane in an atmospheric pressure AC gliding arc discharge: Co-generation of syngas and carbon nanomaterials. *Int. J. Hydrogen Energy* **2014**, *39*, 9658−9669.

(6) Snoeckx, R.; Bogaerts, A. Plasma technology − a novel solution for CO_2 conversion? *Chem. Soc. Rev.* **2017**, *46*, 5805−5863.

(7) Nunnally, T.; Gutsol, K.; Rabinovich, A.; Fridman, A.; Gutsol, A.; Kemoun, A. Dissoaciation of CO_2 in a low current gliding arc plasmatron. *J. Phys. D: Appl. Phys.* **2011**, *44*, 274009.

(8) Kim, S. C.; Lim, M. S.; Chun, Y. N. Reduction characteristics of carbon dioxide using a plasmatron. *Plasma Chem. Plasma Process.* **2014**, *34*, 125−143.

(9) Liu, J.; Park, H.; Chung, W.; Park, D. High-Efficient Conversion of CO_2 in AC-Pulsed Tornado Gliding Arc Plasma. *Plasma Chem. Plasma Process.* **2016**, *36*, 437−449.

(10) Bongers, W.; Bouwmeester, H.; Wolf, B.; Peeters, F.; Welzel, S.; van den Bekerom, D.; den Harder, N.; Goede, A.; Graswinckel, M.; Groen, P.; et al. Plasma-driven dissociation of CO_2 for fuel synthesis. *Plasma Processes Polym.* **2017**, *14*, 1600126.

(11) Gutsol, A.; Bakken, J. A. A new vortex method of plasma insulation and explanation of the Ranque effect. *J. Phys. D: Appl. Phys.* **1998**, *31*, 704−711.

(12) Gutsol, A.; Larjo, J.; Herenberg, R. RF inductive plasma torch with reverse vortex stabilization. *Proceedings of the International Symposium on Plasma Chemistry, Prague, Czech Republic*, 2001; Vol. *14*, p0227.

(13) Trenchev, G.; Kolev, St.; Bogaerts, A. A 3D model of a reverse vortex flow gliding arc reactor. *Plasma Sources Sci. Technol.* **2016**, *25*, 035014.

(14) Ramakers, M.; Trenchev, G.; Heijkers, S.; Wang, W.; Bogaerts, A. Gliding Arc Plasmatron: providing an alternative method for carbon dioxide conversion. *ChemSusChem* **2017**, *10*, 2642−2652.

(15) Menter, F. R.; Kuntz, M.; Langtry, R. Ten Years of Industrial Experience with the SST Turbulence Model, Turbulence. *Heat and Mass Transfer* **2003**, *4*, 625−632.

(16) Weigand, B.; Ferguson, J. R.; Crawford, M. E. An Extended Kays and Crawford turbulent Prandtl number model. *Int. J. Heat Mass Transfer* **1997**, *40*, 4191−4196.

(17) Wang, W.; Berthelot, A.; Kolev, St.; Tu, X.; Bogaerts, A. CO_2 conversion in a gliding arc plasma: 1D cylindrical discharge model. *Plasma Sources Sci. Technol.* **2016**, *25*, 065012.

(18) Comsol Multiphysics, version 5.0; User's Guide, 2015; www.comsol.com (accessed December 2015).

(19) Ferziger, J. H.; Peri'c, M. *Computational Methods for Fluid Dynamics*, 3rd ed.; Springer-Verlag: Germany, 2002.

(20) Kolev, St.; Bogaerts, A. A 2D model for a gliding arc discharge. *Plasma Sources Sci. Technol.* **2015**, *24*, 015025.

(21) Kolev, St.; Sun, S.; Trenchev, G.; Wang, W.; Wang, H.; Bogaerts, A. Quasi-neutral modeling of gliding arc plasmas. *Plasma Processes Polym.* **2017**, *14*, 1600110.

(22) Sun, S. R.; Wang, H.; Mei, D. H.; Tu, X.; Bogaerts, A. CO_2 conversion in a gliding arc plasma: Performance improvement based on chemical reaction modelling. *Journal of CO_2 Utilization* **2017**, *17*, 220−234.

(23) Berthelot, A.; Bogaerts, A. Modeling of plasma-based CO_2 conversion: lumping of the vibrational levels. *Plasma Sources Sci. Technol.* **2016**, *25*, 045022.

(24) Kozák, T.; Bogaerts, A. Splitting of CO_2 by vibrational excitation in non-equilibrium plasmas: a reaction kinetics model. *Plasma Sources Sci. Technol.* **2014**, *23*, 045004.

(25) Kozák, T.; Bogaerts, A. Evaluation of the energy efficiency of CO_2 conversion in microwave discharges using a reaction kinetics model. *Plasma Sources Sci. Technol.* **2015**, *24*, 015024.

(26) Czernichowski, A.; Nassar, H.; Ranaivosoloarimanana, A.; et al. Spectral and electrical diagnostics of gliding arc. *Acta Phys. Pol., A* **1996**, *89*, 595−603.

(27) Zhukov, M. F.; Zasypkin, I. M. *Thermal Plasma Torches Design, Characteristics, Applications*; CISP Ltd.: Cambridge, UK, 2007.

(28) Ramakers, M.; Medrano, J.; Trenchev, G.; Gallucci, F.; Bogaerts, A.; Revealing the arc dynamics in a Gliding Arc Plasmatron: A better insight to improve gas conversion applications, (submitted to *Plasma Sources Sci. Technol.*, under review).

(29) Sun, S. R.; Kolev, St.; Wang, H. X.; Bogaerts, A. Coupled gas flow-plasma model for a gliding arc: investigations of the back-breakdown phenomenon and its effect on the gliding arc characteristics. *Plasma Sources Sci. Technol.* **2017**, *26*, 015003.

(30) Nunnally, T. Application of low current gliding arc plasma discharges for hydrogen sulfide decomposition and carbon dioxide emission reduction. PhD Thesis, Drexel University, 2011.

(31) Gangoli, S. P. Design and preliminary characterization of the magnetically stabilized gliding arc. Master Thesis, Drexel University, 2007.

(32) Berthelot, A.; Bogaerts, A. Modeling of CO_2 Splitting in a Microwave Plasma: How to Improve the Conversion and Energy Efficiency. *J. Phys. Chem. C* **2017**, *121*, 8236−8251.

DOI: 10.1021/acs.jpcc.7b08511
J. Phys. Chem. C XXXX, XXX, XXX−XXX